lajss.org© Latin American Journal of Solids and Structures
www.lajss.org

Analysis of stress concentration in pseudoelastic plates using digital image correlation (DIC) and finite element method

Bruno Felippe Silva [a,b*], Luís Felipe Guimarães de Souza [a], Ricardo Alexandre Amar de Aguiar [a], Pedro Manuel Calas Lopes Pacheco [a]

[a] CEFET/RJ, Department of Mechanical Engineering - Programa de Pós-Graduação em Engenharia Mecânica e Tecnologia de Materiais (PPEMM). Email: bfsilva@anp.gov.br, luis.souza@cefet-rj.br, ricardo.aguiar@cefet-rj.br, pedro.pacheco@cefet-rj.br
[b] ANP - Brazilian National Agency for Petroleum, Natural Gas and Biofuels.

* Corresponding author

https://doi.org/10.1590/1679-7825/e8703

Abstract

Shape Memory Alloys (SMAs) are materials known for their thermomechanical coupling associated to phase transformation processes. When subjected to stresses, SMAs exhibit nonlinear characteristics, necessitating special methodologies to assess their performance and structural integrity. The design of mechanical components with geometric discontinuities, such as notches and holes, has traditionally been addressed through simplified mechanical design methods incorporating stress concentration factors (SCFs). These approaches are applied under both static and cyclic mechanical or thermal loading conditions. The presence of plastic deformations introduces stress/strain redistribution and nonlinearities effects such as plasticity. In this work the stress concentration in SMA pseudoelastic thin plates with holes is investigated through numerical simulations and experimental tests. The numerical model is based on finite elements method using a SMA constitutive model to represent the pseudoelastic behavior and plasticity is calibrated from experimental results obtained from tension tests with the Digital Image Correlation (DIC) method. The numerical results present the effect of stresses and martensitic volume fractions and the strain decomposition results considering elasticity, phase transformation and plasticity. An experimental-numerical calibration is performed with good agreement. The DIC results present a Lüders type strain related to the preferential transformation pattern. The stress concentration factors are calculated from numerical results and show a variation of its value according to the stage of phase transformation and plasticity. The study presents a proposal of a method to consider the effect of geometry and material properties and load history on the design of mechanical components.

Keywords

shape memory alloys (SMA), pseudoelasticity, stress concentration, finite element method, digital image correlation

Received May 08, 2025. In revised form July 25, 2025. Accepted August 24, 2025. Available online August 27, 2025.
https://doi.org/10.1590/1679-7825/e8703

Graphical Abstract

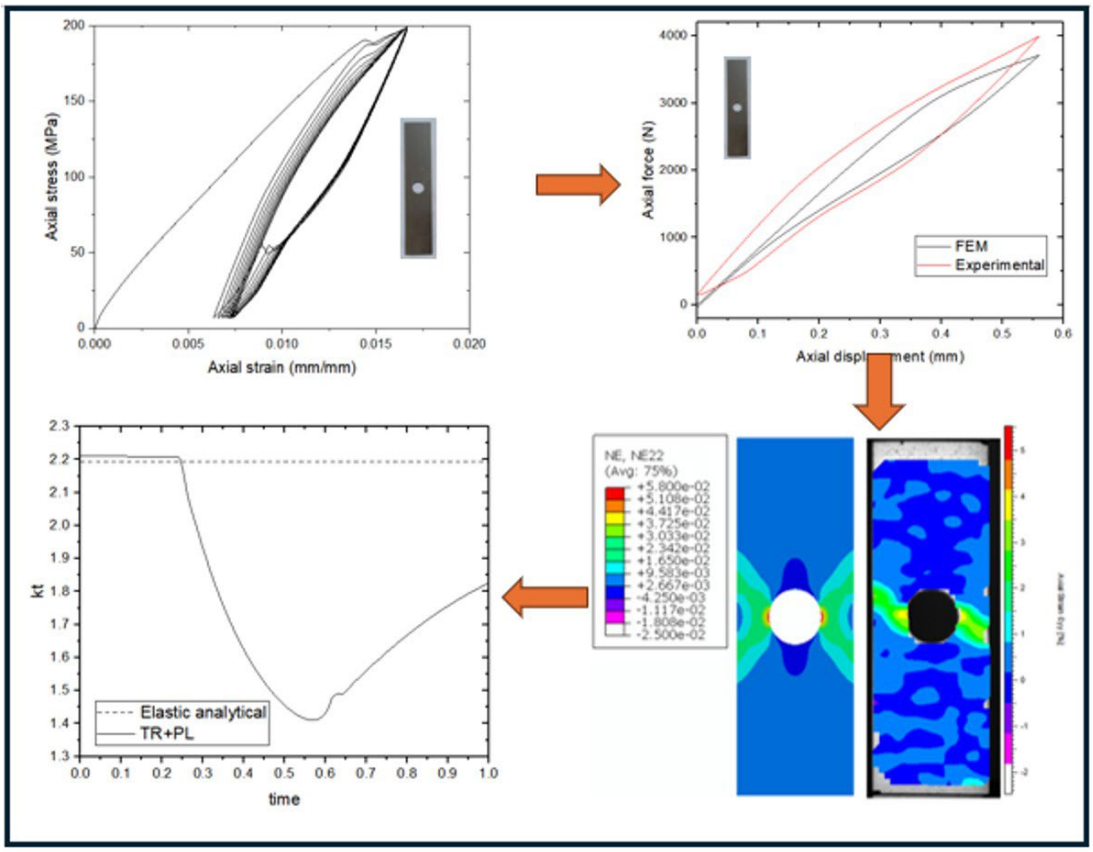

1 INTRODUCTION

Shape memory alloys (SMAs) are versatile, multifunctional materials that serve as both structural components and possess additional functionalities, such as performance enhancement, sensing capabilities, and electromagnetic sealing (Lagoudas, 2008). They are notable for their ability to convert non-mechanical signals, such as thermal or magnetic stimuli, into mechanical responses.

Among the various types of SMAs, nickel-titanium (NiTi) alloy is widely utilized (Lecce, 2015) and is the focus of this study. The shape memory effect in NiTi arises from phase transformations between two main phases: austenite, which has a simpler and more ordered crystalline structure stable at high temperatures in a stress-free state, and martensite, which has a more complex crystalline structure stable at low temperatures in a stress-free state (Lagoudas, 2008).

Pseudoelastic behavior occurs at temperatures above the austenite finish temperature (A_f). Under mechanical loading, the alloy undergoes a transformation to un-twinned martensite, followed by a complete reversal of deformation and a return to the austenite phase during unloading (Lagoudas, 2008).

Understanding stress concentration factors (SCF) in notched mechanical components is important for determining part dimensions and understanding crack initiation and propagation, as emphasized by Simoes and Martínez-Pañeda (2021) and Hasan and Baxenavis (2019). Stress concentration also affects damage behavior (Phillips et al., 2019).

There are several analytical solutions for stress concentration factors in the linear elastic regime, such as the Kirsch problem (Pilkey, Walter, 1997), which examines the stress field in an infinite plate with a circular hole subjected to uniaxial stress applied far from the hole. The Kirsch analytical solution predicts a stress concentration factor of 3, corresponding to the maximum stress observed at the edge of the hole in an infinite linear-elastic plate. However, the value of k_t changes for finite plates when the effect of the plate's edge is considered. Similar values of strain concentration are also observed.

In the elastoplastic regime, which can occur near geometric discontinuities, the stress concentration factor differs from that calculated for the linear-elastic regime. After yielding, the stress concentration factor k_σ decreases, while the strain concentration factor k_ε increases (Castro and Meggiolaro, 2009). This behavior is attributed to the redistribution of the stress field in the region near the geometric discontinuity.

Several studies deal with the problem of measuring the strain fields in shape memory alloys as reported by Shayanfard et al. (2021) and Delpueyo et al. (2021), while others study SMA with notches for designing parts with complex geometries (Paul et al. 2020, Golasiński et al. 2024, Gu et al. 2024, Zitouni et al. 2023).

Numerous studies in the literature address stress concentration in thin pseudoelastic plates with holes. Murasawa et al. (2011) used Brinson's constitutive model (Brinson et al.,1993) to simulate the behavior of a 1 mm thick pseudoelastic plate with double U-shaped notches. They experimentally evaluated the stress-strain behavior in both notched and un-notched sections, analyzing differences between experimental and numerical stress-strain curves. They found that these differences were associated with local strain bands present during stress-induced transformation.

Zhu et al. (2013) conducted a study on thin NiTi plates with various hole arrangements using the Stebner-Brinson model to simulate stress distribution and martensite fractions. They concluded that the number and distribution of holes can affect stress, strain, and phase transformation behaviors. They also highlighted the necessity of considering plasticity for a proper analysis. A subsequent paper by Zhu et al. (2014) included plasticity effects in the study of pseudoelastic plates with different hole configurations. This study described limitations of the constitutive model and concluded that closely spaced holes lead to more evenly distributed stresses, while dispersed holes result in higher localized plasticity effects. Numerical results were compared with experimental values from the literature, which used digital image correlation (DIC) techniques to study axial and transverse strain fields. These fields were used to calculate localized deformation in different regions of the specimen, correlating with phase transformation and demonstrating the technique's effectiveness for this type of research.

Shariat (2014) conducted numerical simulations with different hole sizes, spacings, and orientations, finding that deformation behavior depends on the number and size of the holes. A subsequent study (Shariat, 2014) proposed a constitutive model (calibrated with experimental data) that presents the stress-strain curves of pseudoelastic plates with varying numbers of holes. This study concluded that the plate exhibits a stress gradient during martensitic transformation and found that increasing the hole size expands the stress gradient range. Further experimental tests by Shariat et al. (2014) led to an analytical formulation describing the stress-strain curve. Yao Xiao (2016) studied the effect of double-edge semicircular notches in superelastic NiTi plates, concluding that deeper notches result in greater localized deformations and more evident phase transformation profiles.

Hosseini and Ashrafi (2022) conducted finite element simulations using a constitutive model that considers martensitic transformation and plasticity to calculate the stress concentration factor in pseudoelastic plates. They concluded that when the stress reaches the yield limit, the stress concentration factor decreases.

Using finite element modeling, Silva et al. (2023, 2024a-b, 2025) examined how phase transformations lead to stress redistribution in thin sheets with stress concentrators under cyclic loading. They introduced novel criteria for evaluating stress and strain concentration factors. Their research demonstrated that heat treatment significantly affects the cyclic stress–strain response—particularly the development of a stabilized hysteresis loop following material training—by altering the critical stress levels and transformation temperatures.

The main goal of this study is to evaluate the strain fields using both the finite element method (FEM) and the digital image correlation method (DIC). It aims to analyze the influence of stresses, strains, and martensitic transformations on the stress concentration factors (SCFs).

2 MATERIAL CHARACTERIZATION

The specimen was obtained from a pseudoelastic equiatomic NiTi sheet (acquired from Nexmetal Corporation) according to the ASTM E8 standard (2007), with 1 mm thickness, 100 mm width, and a total length of 200 mm. The specimen was prepared by wire electrical discharge machining, followed by heat treatment at 530°C for 10 minutes, with rapid cooling in water, the heat treatment was necessary due to the limited pseudoelastic behavior of the as-received specimen. Differential Scanning Calorimetry (DSC) analysis (Netzsch DSC200 F3) was performed to determine the transformation temperatures: A_s: -20.1°C, A_f: 1.6°C, R_s: -10.3°C, R_f: -36.8°C, M_s: -51.7°C, and M_f: -77.3°C (Fig. 1), where A_s, A_f, R_s, R_f, M_s, M_f are, respectively, the austenite start transformation temperature, austenite finish transformation temperature, R-phase start transformation temperature, R-phase finish transformation temperature, martensite start transformation temperature, and martensite finish transformation temperature. For the DSC test, a temperature range between -150 and 120°C was used, with a constant heating/cooling rate of 10 °C/min (Fig.1).

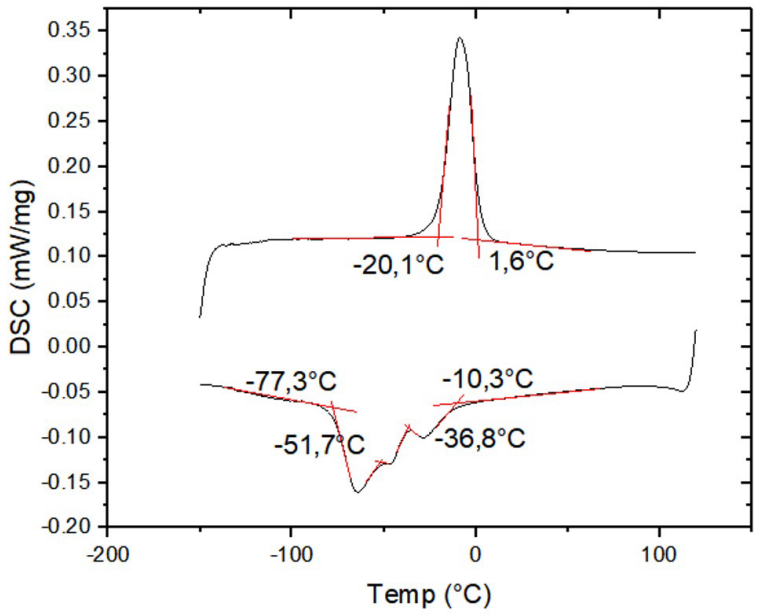

Figure 1 DSC results for the specimen after heat treatment.

One dog bone specimen with a geometry according to the ASTM E8 standard (ASTM, 2007), was tested in an Instron model 5985 universal testing system equipped with a 50 kN load cell at room temperature. A prescribed displacement was applied through a sequence of quasi-static triangular loading at a rate of 1%/min. The strain was measured using an AVE 2 non-contact video extensometer. Figure 2 presents the experimental setup including the camera for video extensometer and DIC measurement, a drawing of specimen with dimensions and an image of the specimen with two marks spaced 25 mm apart used for the video extensometer measurement.

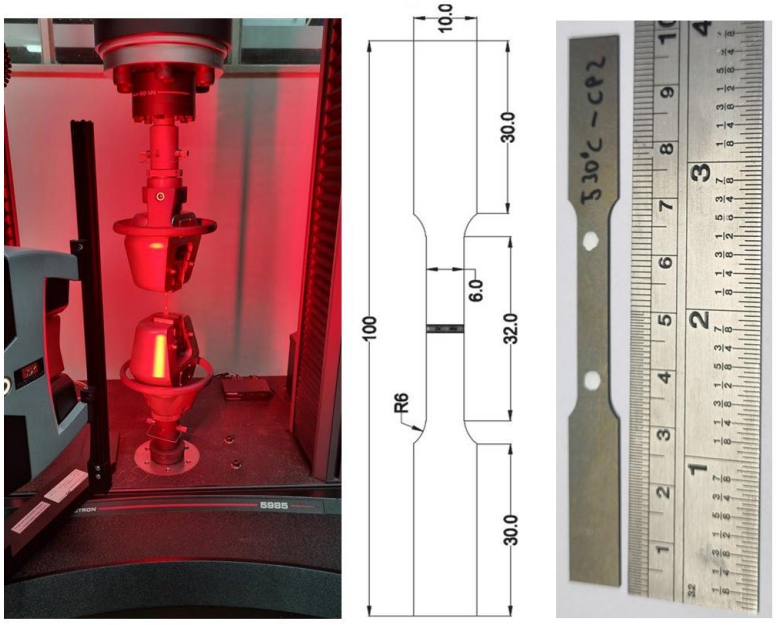

a) b) c)

Figure 2 Experimental setup for the tensile test: a) testing system with an AVE 2 non-contact video extensometer, b) ASTM E8 specimen drawing with dimensions in mm, c) specimen after the heat treatment with two marks for video extensometer measurement

Ten cycles were applied until reaching 6.5% strain and then unloaded to 7 MPa (to avoid compressive residual stresses) after, 1 cycle until 15% were applied followed by the unload until the stress reaches 7 MPa, finally it was applied one last load until fracture. The engineering stress-strain curve of the complete test is presented in Fig. 3.

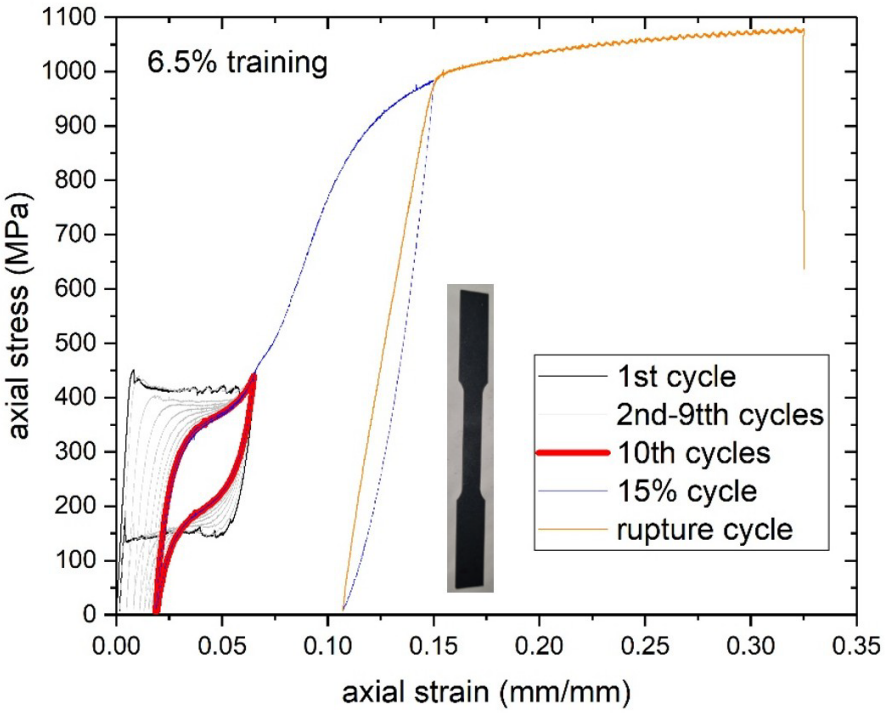

Figure 3 ASTM E8 specimen cyclic engineering Stress-Strain Curve (Silva et al. 2025).

Another specimen of the plate. with 100 mm length and 20 mm width, containing a 9 mm diameter hole at the center was tested by applying 10 cycles of training with the same strain rate as the previous test. The drawing with dimensions is present on Fig. 4a and the picture of the specimen with speckles for DIC measurement is shown in Fig 4b.

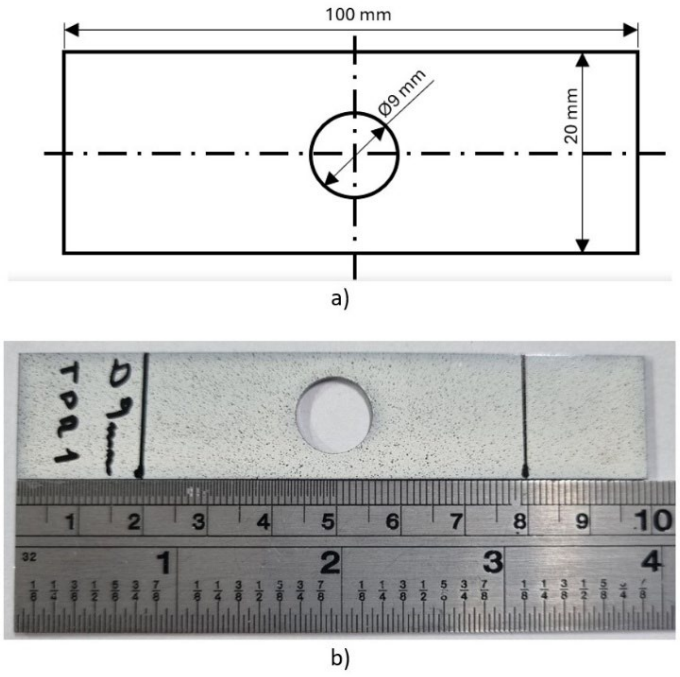

Figure 4 DIC specimen: a) drawing with dimensions, b) picture of specimen with speckles for DIC measurement

The axial engineering stress-strain curve is presented on Fig. 5. There is a relevant transformation induced plasticity (TRIP) behavior in the first cycle and from the second cycle the residual strains are very close.

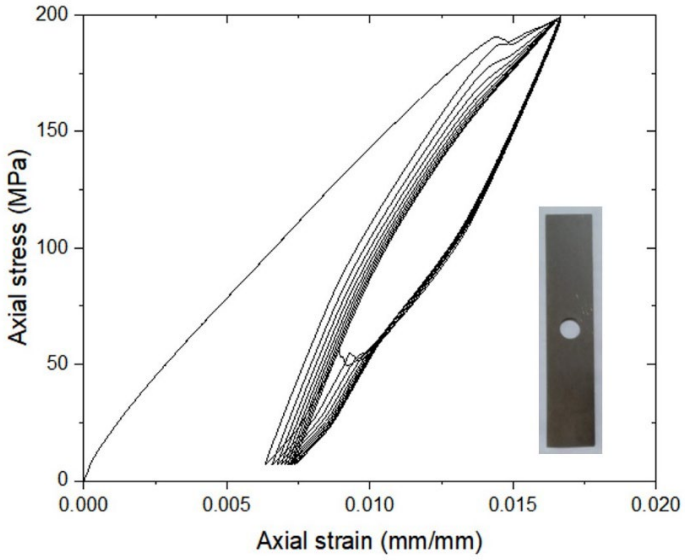

Figure 5 Cyclic Stress-Strain Curve.

3 NUMERICAL MODEL

To simulate the stress-induced transformation process, the Auricchio model (1996) is used. This model considers isothermal pseudoelasticity and employs the Drucker-Prager criterion to describe the critical stresses for pseudoelastic transformation (Lagoudas, 2008). The model also incorporates the effect of plasticity after the martensite transformation reaches the yield limit. The formulation, implemented in the Abaqus computational package (Abaqus, 2018), is based on the additive decomposition of strains, where the total strain is found by summing the elastic, transformation, and plastic components (Lecce, 2015):

$$\Delta\varepsilon = \Delta\varepsilon^{el} + \Delta\varepsilon^{tr} + \Delta\varepsilon^{pl} \tag{1}$$

where $\Delta\varepsilon$, $\Delta\varepsilon^{el}$, $\Delta\varepsilon^{tr}$ and $\Delta\varepsilon^{pl}$ are the total, elastic, phase transformation, and plastic strain increments, respectively.

The constitutive model considers that the modulus of elasticity and Poisson's ratio under intermediate transformation conditions follow the rule of mixtures:

$$E = E_A + \varsigma(E_M - E_A) \tag{2}$$

$$\nu = \nu_A + \varsigma(\nu_M - \nu_A) \tag{3}$$

where E, E_A, E_M, ν, ν_A, ν_M e ς represent, respectively, the resultant modulus of elasticity, the modulus of elasticity of austenite, the modulus of elasticity of martensite, the resultant Poisson's ratio, the Poisson's ratio of austenite, the Poisson's ratio of martensite, and the volume fraction of martensite.

The parameters of the constitutive model are presented in Tables 1 (phase transformation) and Table 2 (plasticity), where ε_r, σ^S_{tL}, σ^E_{tL}, σ^S_{tU}, σ^E_{tU}, σ^S_{cL}, T_0, C_A, C_M are, respectively, the residual strain, the stress at the start of transformation during loading, the stress at the end of transformation during loading, the stress at the start of transformation during unloading, the stress at the end of transformation during unloading, the reference temperature, and the coefficients of stress influence on the transformation temperatures of austenite and martensite. More details about the use of this model and the calibration process can be found in Silva et al. (2025).

Table 1 Parameters of the phase transformation constitutive model

E_A (MPa)	ν_A	E_M (MPa)	ν_M	ε_r	σ^S_{tL} (MPa)	σ^E_{tL} (MPa)	σ^S_{tU} (MPa)	σ^E_{tU} (MPa)	σ^S_{cL} (MPa)	T_0 (K)	C_A (MPa/K)	C_M (MPa/K)
30180	0.3	25000	0.3	0.018	250	408	272	50	250	323	7	6.5

The constitutive model parameters associated with plastic behavior are presented in Table 2 and consist of stress and strain values obtained at 3 points of the experimental test in the plastic region of the stress-strain curve.

Table 2 – Plasticity parameters for the constitutive model

Stress **(MPa)**	**Total strain (mm/mm)**
745	0.08
880	0.1
1072	0.3

The calibration process for the constitutive model parameters considers the stabilized cycle (the tenth cycle up to 6.5% strain, the cycle with 15% strain, and the load up to 30%). Figure 6 shows a good correspondence between the curve obtained with the model and the experimental curve.

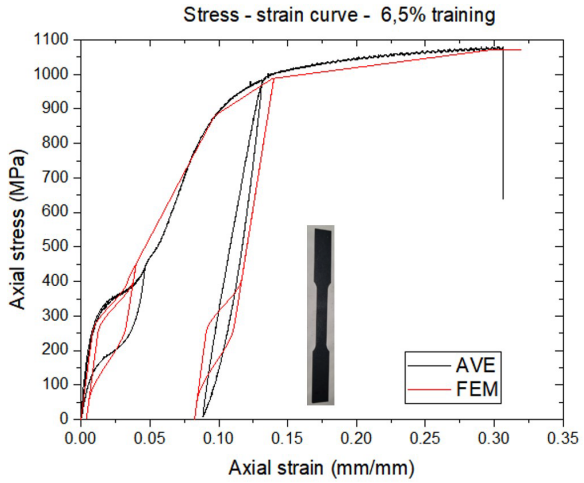

Figure 6 Comparison between the curve obtained with the numerical model and the experimental curve.

To study stress concentration, a finite element model was developed for a plate with a width of 20 mm, a length of 100 mm, and a central hole with a diameter of 9 mm. For the sake of simplifying the model, a double symmetry was used. The mesh, obtained after a convergence analysis, consists of 629 CPS8 elements (quadratic plane stress elements) and 2004 nodes. A representation of the specimen with symmetry boundary conditions and the vertical loading displacement applied is presented in Fig. 7 where u_{11} stands for horizontal displacement and u_{22} for vertical displacement.

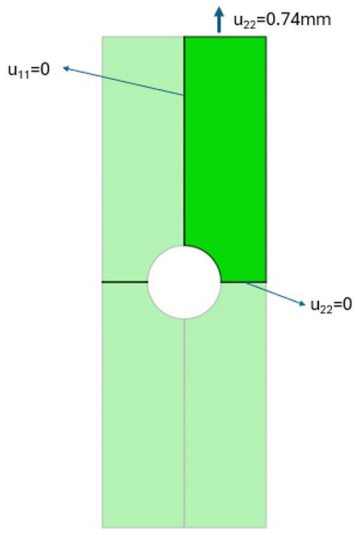

Figure 7 Model representation of symmetry, boundary conditions and loading

The calibration of the FEM model with the 10° cycle of the experiment is presented on Fig. 8. The initial load value is near to 200 N because the unload of the previous finished at 7 MPa. Both curves show an adequate relation.

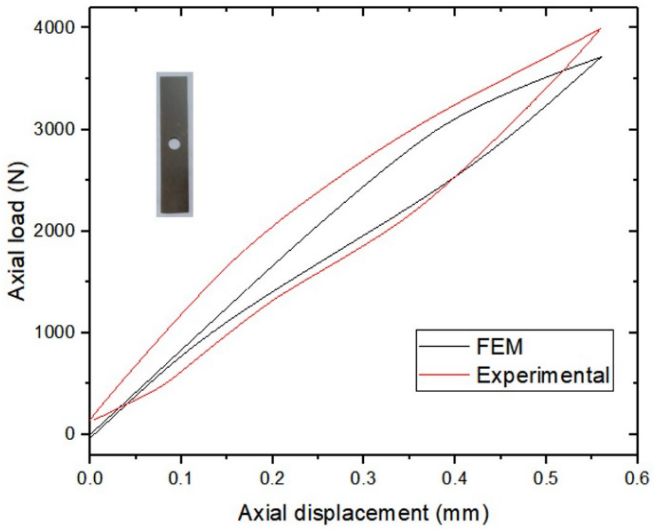

Figure 8 Experimental and FEM axial load x displacement curve.

The axial strain results of FEM (Fig 9a) and Digital image correlation (Fig 9b) are presented in Fig. 9 for the maximum axial load displacement condition. A good agreement for the maximum strain values is observed. Both results present higher values around the hole that spread at 45°.

The axial strain results obtained through the finite element method (FEM) indicate a higher strain at the edge of the hole, with a maximum value of 5.49% in a highly localized area. This strain region expands in an "X" shape (Fig. 9a), from the center of the hole, it relates to the region of maximum shear stress where the stress levels are high enough to initiate phase transformation into pseudoelastic materials. In contrast, the experimental results for the same displacement show that deformation initially occurred at an inclined line (Fig. 9b). This difference is attributed to the formation of Lüders bands, which are localized strain bands (He, 2023), however the constitutive model used in the simulation does not capture this phenomenon.

From the beginning of the load application, stress concentration points form at the edge of the hole, but there is no austenite transformation. As the sample reaches a critical stress value, the phase transformation begins. Then, as the stress continues to increase, the sample reaches the yield point, triggering the plasticity effect. The numerical model was represented with ¼ symmetry for simplification (after a prior verification with a full geometry representation), and the result is completely symmetric, since the constitutive model does not capture this behavior, as it calculates strain considering the symmetry condition.

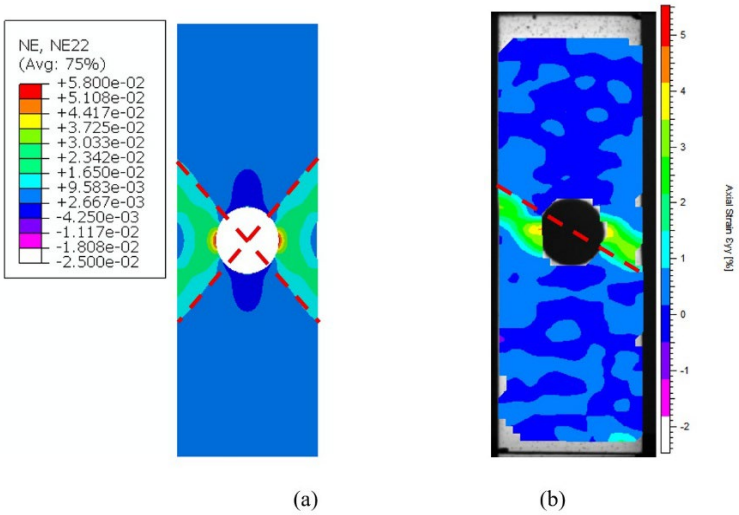

Figure 9 Maximum displacement loading condition: a) FEM axial strain (mm/mm), b) DIC axial strain (%).

The same phenomena occur at axial strain results presented on Fig. 10. Despite the resolution issues related to the axial results, the results show a good agreement between FEM and DIC results although the experimental results present some perturbations across the part (in places distant from the hole), this is caused by the interpolation strain values in some regions. The minimum strain value at 45° has a magnitude of -1.6%.

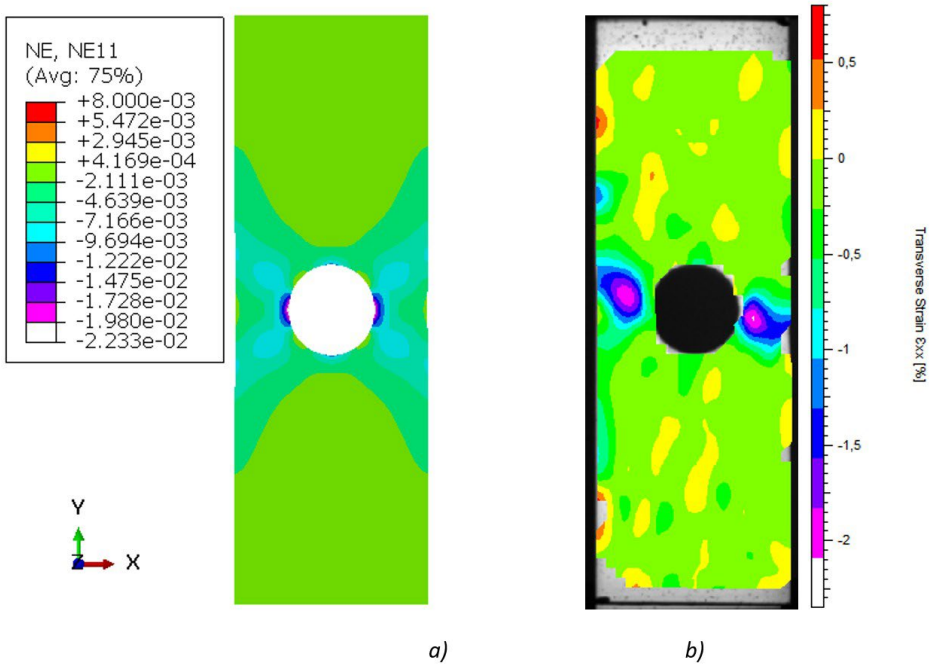

Figure 10 Maximum displacement loading condition: a) FEM shear stress (mm/mm) b) DIC axial strain (%).

The martensitic volumetric fraction (MVF) and the axial stress of FEM method are presented in Fig. 11a. The MVF result shows a partial transformation around the hole. As expected, the axial stress (Fig. 11b) presents a maximum value at the same region around the hole.

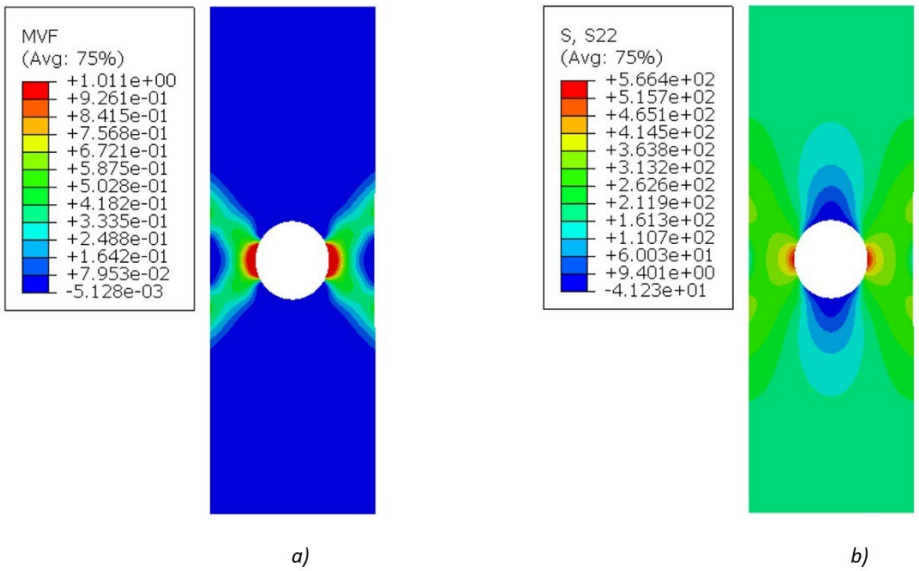

Figure 11 Maximum displacement loading condition: a) Martensitic volumetric fraction (MVF) b) axial stress (MPa).

Stress concentration factor evolution during the loading steps is present on Fig. 12, where the horizontal dashed line indicates the analytical elastic SCF value while the solid line indicates the pseudoelastic result obtained from de FEM analysis considering plasticity and phase transformation. The FEM SCF value is calculated as the ratio between the maximum stress value and the nominal stress (considering the width discounting the diameter). In the beginning of the

load the SCF is constant and similar to the analytic value, as the material is completely austenitic in an elastic region. When the phase transformation begins, the SCF reduces until martensitic phase transformation expands for a larger area. Finally, the SCF experiments a rise. This complex behavior is difficult to observe in traditional experimental tests and the use of experimental methods such as DIC in combination with numerical simulations are necessary to allow a local analysis of the large strains present associated with the phase transformation phenomenon.

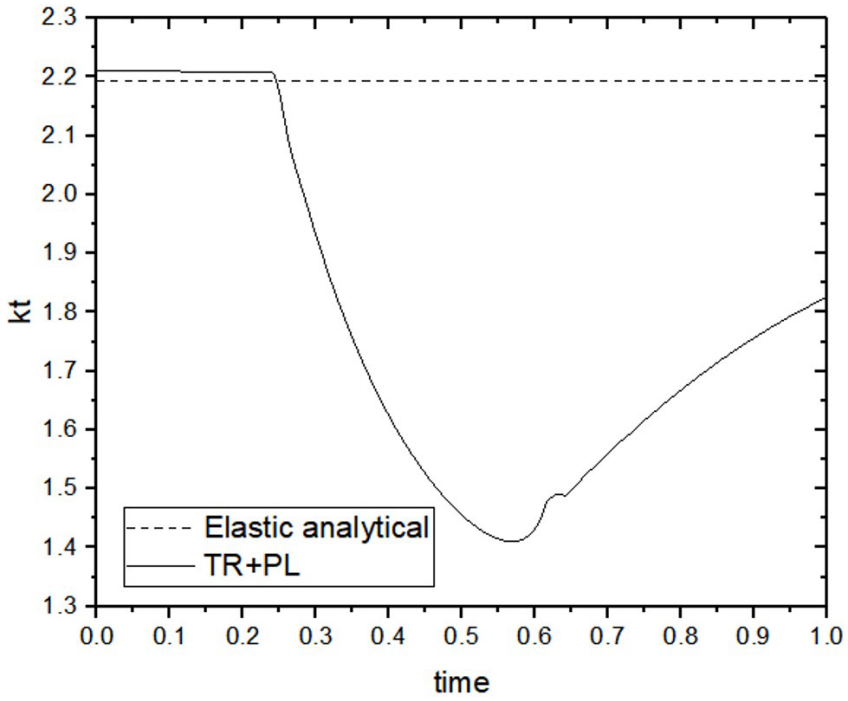

Figure 12 Evolution of the Stress Concentration Factor (SCF) during loading for elastic analytic and FEM results.

4 CONCLUSIONS

The behavior of the stress concentration factor (SCF) in thin pseudoelastic plates is a complex topic that warrants specific studies. This work presents a study on the influence of plasticity in thin pseudoelastic plates with a hole, using a numerical model based on the finite element method that considers a constitutive model for pseudoelastic materials with phase transformation and plasticity. The numerical model has been compared to experimental results with good agreement.

The numerical results indicate the influence of the geometric discontinuity on the strain fields which reflects on stress and martensitic transformation.

The digital image correlation (DIC) technique enables the acquisition of the full strain field in various directions and allows the analysis of complex behaviors such as pseudoelasticity. Although the DIC results show good agreement with the finite element method (FEM) simulations, a more in-depth study is necessary to fully compare and validate these two approaches.

The stress concentration factor was calculated from numerical results and presented a specific behavior as follows: initially the SCF is constant, followed by a reduction after the beginning of transformation, when a certain point when a higher portion of the specimen is transformed, after the yielding it happens a reduction of the curve slope related to plasticity.

The complex behavior of the stress concentration factor in pseudoelastic parts is difficult to observe experimentally. Therefore, it is necessary to study experimental methods, such as digital image correlation, to enable numerical methods (e.g., FEM) to produce reliable results. The use of classic design approaches in shape memory alloys indicate a more simple and reliable way to study parts with complex geometries.

ACKNOWLEDGMENT

The authors would like to acknowledge the support of CEFET/RJ and the Brazilian Research Agencies CNPq, Capes, Faperj, INCT-EIE of Smart Structures in Engineering and Finep.

Author's Contributions: Conceptualization, BF Silva, LFG Souza, RAA Aguiar, PMCL Pacheco; **Methodology**, BF Silva, LFG Souza, RAA Aguiar, PMCL Pacheco; **Investigation**, BF Silva, LFG Souza, RAA Aguiar, PMCL Pacheco; **Writing - original draft**, BF Silva, LFG Souza, RAA Aguiar, PMCL Pacheco; **Writing - review & editing**, BF Silva, LFG Souza, RAA Aguiar, PMCL Pacheco;

Data availability statement: Research data is only available upon request

Editor: Eduardo Alberto Fancello and Paulo de Tarso Mendonça

References

ABAQUS (2018) ABAQUS User Manuals, Version

ASTM E8, (2007) Standard Test Methods for Tension Testing of Metallic Materials, ASTM International, 2007

Auricchio, F., and R.L. Taylor, (1996) Shape-Memory Alloys: Modeling and Numerical Simulations of the Finite-Strain Superelastic Behavior, Computer Methods in Applied Mechanics and Engineering.

Brinson L.C. (1993) One-Dimensional Constitutive Behavior of Shape Memory Alloys: Thermomechanical Derivation with Non-Constant Material Functions and Redefined Martensite Internal Variable. Journal of Intelligent Material Systems and Structures.

Castro, J.T.P, Meggiolaro, M. A., (2009) Fatigue Techniques and Sizing Practices under Actual Service Loads. Createspace Independent Publishing Platform.

Delpueyo, D., Jury, A., Balandraud, X., Grédiac, M., (2021) Applying Full-Field Measurement Techniques for the Thermomechanical Characterization of Shape Memory Alloys: A Review and Classification. Shape Memory and Superelasticity. https://doi.org/10.1007/s40830-021-00355-w

Golasiński, K.M., Maj, M., Tasaki, W., Pieczyska, E.A., Kim, H.Y., (2024) Full-Field Deformation Study of Ti–25Nb, Ti–25Nb–0.3O and Ti–25Nb–0.7O Shape Memory Alloys During Tension Using Digital Image Correlation. Metallurgical and Materials Transactions A. https://doi.org/10.1007/s11661-024-07414-8

Gu, X., Cao, Y., Zhu, J., Wang, J., Zhang, W., Moumni, Z., (2020) Shape optimization of SMA structures with respect to fatigue, Materials & Design, 2020, https://doi.org/10.1016/j.matdes.2019.108456.

Hasan, M. M., Baxevanis, T., (2019) Actuation Fatigue Life Prediction of Notched Shape Memory Alloy Members. Journal of Applied Mechanics.

He, Y.J., (2023) Interface propagation and energy dissipation in Shape Memory Alloys, Scripta Materialia, https://doi.org/10.1016/j.scriptamat.2023.115420.

Hosseini S.M., Ashrafi M.J., (2023) Stress concentration in shape memory alloy sheets with circular cavities: Effects of transformation, saturation, and plasticity. The Journal of Strain Analysis for Engineering Design. 2023

Lagoudas, D., (2008) Shape memory Alloys, Springer.

Lecce, L., (2015) Shape Memory Alloy engineering for Aerospace, Structural and Biomedical Applications. Elsevier.

Murasawa, G., Yoneyama, S., Miyata, K., Nishioka, A. and Koda, T., (2011) Finite Element Analysis and Experimental Measurement of Deformation Behavior for NiTi Plate With Stress Concentration Part Under Uniaxial Tensile Loading. Strain.

Paul, P.P., Paranjape, H. M., Amin-Ahmadi, B., Pagan, D.C., Chumlyakov, Y. I., Brinson, L. C., (2020) Heterogeneity and inelasticity of deformation in a notched martensitic NiTi shape memory alloy specimen, Acta Materialia, https://doi.org/10.1016/j.actamat.2020.05.019.

Phillips, F. R., Wheeler, R.W., Geltmacher, A. B., Lagoudas D. C., (2019) Evolution of internal damage during actuation fatigue in shape memory alloys. International Journal of Fatigue.

Pilkey, Walter D., (1997) Peterson's stress concentration factors, John Wiley & Sons, Inc.

Housseini S. M., Ashrafi, M. J., (2022) Stress concentration in shape memory alloy sheets with circular cavities: Effect of transformation, saturation and plasticity. Journal of strain analysis.

Silva B.F., Souza L.F.G., Aguiar, R.A.A., Pacheco P.M.C.L., (2023) Analysis of stress concentration in pseudoelastic thin sheets using the finite element method, Proceedings COBEM 2023. DOI://10.26678/ABCM.COBEM2023.COB2023-0759

Silva B.F., Souza L.F.G., Aguiar R.A.A., Pacheco P.M.C.L., (2024a) Análise por Elementos Finitos do Fator de Concentração de Tensão em uma Chapa Fina Pseudoelástica com Transformação de Fase e Plasticidade, Proceedings CONEM 2024, (in Portuguese). DOI://10.26678/ABCM.CONEM2024.CON24-1178.

Silva B.F., Souza L.F.G., Aguiar R.A.A., Pacheco P.M.C.L., (2024b) Analysis of stress concentration in pseudoelastic plates using digital image correlation (DIC) and finite element method, Proceedings Mecsol 2024. DOI://10.26678/ABCM.MECSOL2024.MSL24-0101.

Silva B.F., Souza L.F.G., Aguiar, R.A.A., Pacheco P.M.C.L., (2025) “Analysis of stress concentration in pseudoelastic thin sheets using the finite element method, Journal of the Brazilian Society of Mechanical Sciences and Engineering”, 47:408, https://doi.org/10.1007/s40430-025-05715-6

Simoes, M.; Martínez-Pañeda, E., (2021) Phase field modelling of fracture and fatigue in Shape Memory Alloys. Computer Methods in Applied Mechanics and Engineering.

Shariat, B. S., Liu, Y., Rio, G., (2013) Finite element computational modelling and experimental investigation of perforated NiTi plates under tension, Materials Research Bulletin.

Shariat, B. S., (2014) Pseudoelastic behaviour of perforated NiTi shape memory plates under tension. Intermetallics.

Shariat BS, Liu Y, Rio G., (2014) Numerical modelling of pseudoelastic behaviour of NiTi porous plates. Journal of Intelligent Material Systems and Structures.

Shayanfard, P., Alarcon, E., Barati, M., Mahtabi, M. J., Kadkhodaei, M., Arbab Chirani, S., & Šandera, P. (2021). Stress raisers and fracture in shape memory alloys: review and ongoing challenges. Critical Reviews in Solid State and Materials Sciences, 2021. https://doi.org/10.1080/10408436.2021.1896475

Xiao, Y., Zeng, P., Lei, L., (2016) Effect of double-edge semi-circular notches on the mechanical response of superelastic NiTi shape memory alloy: Experimental observations. The Journal of Strain Analysis for Engineering Designs.

Zhu, P., Stebner, A. P., Brinson, C., (2013) A numerical study of the coupling of elastic and transformation fields in pore arrays in shape memory alloy plates to advance porous structure design and optimization, Smart Materials and Structures.

Zhu, P., Stebner, A. P., Brinson, C., (2014) Plastic and transformation interactions of pores in shape memory alloy plates. Smart Materials and Structures.

Zitouni, I., Abuzaid, W., Egilmez, M., Alkhader, M., (2023) Experimental assessment of the functional fatigue in biocompatible Ti67Zr19Nb11.5Sn2.5 shape memory alloy in the vicinity of drilled holes, Journal of Materials Research and Technology, https://doi.org/10.1016/j.jmrt.2023.10.143.